

GWSkyNet II : a refined machine learning pipeline for real-time classification of public gravitational wave alerts

MAN LEONG CHAN,¹ JESS MCIVER,¹ ASHISH MAHABAL,^{2,3} CODY MESSICK,⁴ DARYL HAGGARD,^{5,6} NAYYER RAZA,^{5,6}
YANNICK LECOEUICHE,¹ PATRICK J. SUTTON,⁷ BECCA EWING,^{8,9} FRANCESCO DI RENZO,¹⁰ MIRIAM CABERO,¹
RAYMOND NG,¹¹ MICHAEL W. COUGHLIN,¹² SHAON GHOSH,¹³ AND PATRICK GODWIN¹⁴

¹*Department of Physics and Astronomy, The University of British Columbia, Vancouver, BC V6T 1Z4, Canada*

²*Division of Physics, Mathematics and Astronomy, California Institute of Technology, Pasadena, CA 91125, USA*

³*Center for Data Driven Discovery, California Institute of Technology, Pasadena, CA 91125, USA*

⁴*University of Wisconsin-Milwaukee, Milwaukee, WI 53201, USA*

⁵*Department of Physics, McGill University, 3600 rue University, Montreal, Quebec H3A2T8, Canada*

⁶*Trottier Space Institute at McGill, 3550 rue University, Montreal, Quebec H3A2A7, Canada*

⁷*Gravity Exploration Institute, Cardiff University, Cardiff CF24 3AA, UK*

⁸*Department of Physics, The Pennsylvania State University, University Park, PA 16802, USA*

⁹*Institute for Gravitation and the Cosmos, The Pennsylvania State University, University Park, PA 16802, USA*

¹⁰*Université Lyon, Université Claude Bernard Lyon 1, CNRS, IP2I Lyon/IN2P3, UMR 5822, F-69622 Villeurbanne, France*

¹¹*Department of Computer Science, University of British Columbia, Vancouver, British Columbia, V6T1Z4, Canada*

¹²*School of Physics and Astronomy, University of Minnesota, Minneapolis, Minnesota 55455, USA*

¹³*Montclair State University, 1 Normal Ave. Montclair, NJ 07043*

¹⁴*LIGO Laboratory, California Institute of Technology, Pasadena, CA 91125, USA*

ABSTRACT

Electromagnetic follow-up observations of gravitational wave events offer critical insights and provide significant scientific gain from this new class of astrophysical transients. Accurate identification of gravitational wave candidates and rapid release of sky localization information are crucial for the success of these electromagnetic follow-up observations. However, searches for gravitational wave candidates in real time suffer a non-negligible false alarm rate. By leveraging the sky localization information and other metadata associated with gravitational wave candidates, **GWSkyNet**, a machine learning classifier developed by Cabero et al. (2020), demonstrated promising accuracy for the identification of the origin of event candidates. We improve the performance of the classifier for LIGO-Virgo-KAGRA’s fourth observing run by reviewing and updating the architecture and features used as inputs by the algorithm. We also retrain and fine-tune the classifier with data from the third observing run. To improve the prospect of electromagnetic follow-up observations, we incorporate **GWSkyNet** into LIGO-Virgo-KAGRA’s low-latency infrastructure as an automatic pipeline for the evaluation of gravitational wave alerts in real time. We test the readiness of the algorithm on a LIGO-Virgo-KAGRA mock data challenge campaign. The results show that by thresholding on the **GWSkyNet** score, noise masquerading as astrophysical sources can be rejected efficiently and the majority of true astrophysical signals correctly identified.

1. INTRODUCTION

The LIGO-Virgo-KAGRA Collaboration (LVK) has so far reported nearly a hundred gravitational wave (GW) events from compact binary coalescences (CBCs) (Abbott et al. 2019, 2021a,c). Sources of GWs such as CBCs involving at least one neutron star may also produce accompanying electromagnetic (EM) emissions. This was demonstrated by the first directly observed binary neutron star (BNS) inspiral by the LIGO Sci-

entific and Virgo Collaboration (LVC), referred to as GW170817 (Abbott et al. 2017a). Simultaneous observations of the GW event and the associated gamma-ray burst triggered an extensive multi-messenger campaign, which resulted in the detection of the associated counterparts across a wide range of X-ray through radio wavelength (Coulter et al. 2017; Smartt et al. 2017; Goldstein et al. 2017; Savchenko et al. 2017; Abbott et al. 2017b; Abbott et al. 2017a).

Coincident EM and GW observations of CBCs involving a neutron star clearly provide valuable information leading to a deeper understanding of the sources. Such observations can help constrain the equation of state of neutron star matter (Radice et al. 2018; Bauswein et al. 2017; Margalit & Metzger 2017; Coughlin et al. 2019a, 2018, 2019b; Annala et al. 2018; Most et al. 2018; Lai et al. 2019; Dietrich et al. 2020; Huth et al. 2022), and provide insights into the central engine of short gamma-ray bursts (Abbott et al. 2017a). A better understanding of the origin of r -process elements in the Universe can also be achieved (Drout et al. 2017; Coulter et al. 2017; Chornock et al. 2017; Cowperthwaite et al. 2017; Pian et al. 2017; Rosswog et al. 2017; Smartt et al. 2017; Watson et al. 2019; Kasliwal et al. 2019). Additionally, such observations can break the modeling degeneracies of the source properties and independently measure the Hubble constant (Abbott et al. 2017b; Coughlin et al. 2020a,b; Hotokezaka et al. 2019; Dietrich et al. 2020).

However, the success of multi-messenger observations of GW sources depends crucially on a number of factors including the sky localization and the rapid release of the GW alerts. The 90% credible region the size of $\mathcal{O}(10)$ to $\mathcal{O}(100)$ deg² can be expected with a large network of GW detectors operating together (Abbott et al. 2018; Petrov et al. 2022; Kiendrebeogo et al. 2023; Pankow et al. 2020). Rapid release of GW alerts, on the other hand, is accomplished with fast data analysis pipelines (Ewing et al. 2024a; Chu et al. 2022a; Nitz et al. 2018; Dal Canton et al. 2021; Adams et al. 2016; Aubin et al. 2021a).

During the third observing run (O3), GW public alerts¹ were released on the Gamma-ray Coordinates Network (GCN)² within minutes of identification by low-latency GW search pipelines, which have built-in tests for the consistency of the phase, amplitude, and timing of candidates in each detector. In O3, a total of 80 alerts were published by the LVK. Of these alerts, however, 24 were subsequently retracted and another 11 were not reported in the offline analyses (Abbott et al. 2021a,c). Some of these alerts had already triggered electromagnetic follow-up observations such as S191213g and S200213t (Antier et al. 2020). This underscores the need for a model capable of reliably determining the origin of GW alerts in real time.

In 2020, Cabero et al. (2020) developed **GWSkyNet**, a machine learning classifier capable of separating GW events from detector noise transients. The classifier was

trained with simulated GW signals from CBCs and non-Gaussian noise transients, known as “glitches”, from **Gravity Spy** collected by the LVC during the first (O1) and second (O2) observing runs (Zevin et al. 2017; Baahadini et al. 2018; Coughlin et al. 2019; Zevin et al. 2023). Assuming GW events with $p_{astro} > 0.5$ as reported by Abbott et al. (2021c); Abbott et al. (2024) are of astrophysical origin, the classifier correctly identified 59 of the 77 CBC public alerts in O3 (assuming a **GWSkyNet** score threshold of 0.75, see section 4), showing promising scientific potential (Cabero et al. 2020). Inspired by the success of **GWSkyNet**, Abbott et al. (2021b) built an extension to the classifier known as **GWSkyNet-Multi**, for the identification of the presence or absence of a neutron star in the source system in addition to noise versus signal classifications. **GWSkyNet-Multi** was reported to show accuracy comparable to **GWSkyNet** (Abbott et al. 2021b). Further study has been undertaken to understand and reveal the inner workings of **GWSkyNet-Multi** (Raza et al. 2024). The results will better inform development of the algorithm and generation of more effective and representative training data.

Given the performance of **GWSkyNet**, the scientific potential of the classifier can be maximized by implementing it as a real-time pipeline for the classification of GW alerts to facilitate potential EM follow-up observations for the fourth observing run (O4). To improve the performance of **GWSkyNet** for O4, we retrain and fine-tune the classifier using the data collected by the LVK during O3. The inputs from a GW candidate to the classifier and the classifier’s architecture are reviewed and updated to be compatible with the alert data expected for public alerts in O4.¹ To demonstrate the readiness of **GWSkyNet**, we participate in a mock data challenge (MDC) (Chaudhary & Toivonen et al. 2023) campaign organized by the LVK.

The paper is organized as follows: In section 2, we provide an overview of the latest changes made to **GWSkyNet**. This includes a discussion of the development of the classifier since its first publication in Cabero et al. (2020). In section 3, we show the readiness and performance of **GWSkyNet** based on the LVK-led MDC campaign. We discuss in section 4 the deployment and implementation of **GWSkyNet** as an automatic pipeline in LVK’s low-latency infrastructure. A summary is given in section 5.

2. GWSkyNet: A MACHINE LEARNING CLASSIFIER

GWSkyNet, developed by Cabero et al. (2020), is a machine learning classifier with a non-sequential

¹ <https://emfollow.docs.ligo.org/>

² <https://gcn.nasa.gov/>

convolutional neural network (CNN) architecture. CNNs are deep learning algorithms commonly used for image classification. In GW astronomy, deep learning algorithms have been applied to the identification of signals and noise (Gabbard et al. 2018; Chan et al. 2020), parameter estimation (Gabbard et al. 2022; Green et al. 2020), sky localization (Chatterjee et al. 2022) and detector noise transient generation (Powell et al. 2023) (for a review, see Cuoco et al. (2020)). Compared to more traditional methods for GW data analysis, an advantage of deep learning algorithms is that they are relatively computationally cheap to run while the performance is comparable (Heaton 2018).

GWSkyNet is designed to distinguish between noise transients and astrophysical signals by leveraging sky localization information and meta data associated with a GW candidate. The features of the data that **GWSkyNet** takes as inputs are mixed, including images and meta data. This allows **GWSkyNet** to evaluate a GW candidate by weighing relevant information with different modalities.

2.1. Inputs and Outputs

For CBC public alerts identified in real time, the LVK generates Flexible Image Transport System (FITS) files containing the sky localization information within seconds to minutes of the identification of the alerts¹ using **BAYESTAR** (Singer & Price 2016; Singer et al. 2016). Information from the FITS files that is important for the identification of the origin of a GW candidate is extracted and used as input to the **GWSkyNet** model. A complete list of the inputs for the current **GWSkyNet** models (Baseline and Fine-tuned models, see sections 2.2 and 2.3) is shown in the right column of Table 1. Also listed in Table 1 are the inputs used by the original **GWSkyNet** model presented in Cabero et al. (2020) for comparison.

GWSkyNet is designed to be a multiple input model consisting of two CNNs and multiple multi-layer perceptrons. Each branch of the ensemble is dedicated to the analysis of a different feature from the input data. The outputs of the branches are concatenated together to form a final prediction. The current architecture of **GWSkyNet** is similar to that shown in Cabero et al. (2020). Several changes are made to the inputs to allow the model to learn a more accurate generalization. First, as stated in Cabero et al. (2020), sky localization of event candidates is extracted and transformed to a 2D projection with 180×360 pixels. However, the 2D projection is no longer down-sampled to 90×180 using maximum pooling. This allows the classifier to learn and perform the down-sampling of the sky local-

ization projection. In addition, instead of utilizing the ansatz location **DISTMU**, the scale parameters **DISTSTD** and the normalization coefficient **DISTNORM** as inputs for space volume localization information, volume reconstruction images are employed. Volume reconstruction images are 2D projections of 3D probability volume map on three planes perpendicular to the principle components of the probability distribution, known as volume rendering images (Singer et al. 2016). The change is made in response to the fact that the values of the normalization coefficient **DISTNORM** from FITS files generated by more recent versions of **BAYESTAR** can be up to 10^{50} , creating increased difficulty for data normalization. Using volume rendering images to describe probability volume map is also consistent with the way public alerts are shown on the gravitational wave-candidate event DataBase (GraceDB).³ For the binary array for the presence and absence of detectors, we adopt a more refined physical definition to better capture event candidate property (see section 2.3). Two other quantities not previously consumed by **GWSkyNet**, the log of the Bayes factors for coherence versus incoherence (**log BCI**) and signal versus noise (**log BSN**) from the FITS files are also used as inputs. As an example, the inputs extracted from the FITS file of a public alert, S191120aj, released in O3 are shown in Figure 1.

Other input information such as the posterior mean distance, the maximum value of GW posterior probability in the sky localization and the normalizing factors for each of the input images are used by both versions of **GWSkyNet**.

By virtue of being a binary classifier, the output from **GWSkyNet** is a class score ranging from 0 (consistent with noise) to 1 (consistent with astrophysical signal) indicating the model’s confidence that the input localization information is internally consistent and aligns with that of a GW signal. We call this score the **GWSkyNet** score for the remainder of the paper. **GWSkyNet** is applicable as long as the sky localization information is produced by **BAYESTAR**. Currently, this is true for **PyCBC** (Nitz et al. 2018; Dal Canton et al. 2021), **GstLAL** (Messick et al. 2017; Tsukada et al. 2023; Ewing et al. 2024b), **SPIIR** (Chu et al. 2022b) and **MBTA** (Aubin et al. 2021b).

2.2. Retraining

Optimal performances of machine learning models are possible only if they are trained on data representative of those expected in practice. Applying a machine learning model to data from a distribution different from that

³ <https://gracedb.ligo.org/>

		Features	
		Cabero et al. (2020)	Baseline and Fine-tuned models
Image inputs		2D sky map (90×180)	2D sky map (180×360)
		DISTMU (90×180)	Vo10 (262×262)
		DISTSTD(90×180)	Vo11 (262×262)
		DISTNORM(90×180)	Vo12 (262×262)
Numerical inputs		A binary array with 3 elements for detectors [†]	A binary array with 3 elements for detectors [†]
		Normalizing factor for the DISTMU image [‡]	Normalizing factor for the Vo10 image [‡]
		Normalizing factor for the DISTSTD image [‡]	Normalizing factor for the Vo11 image [‡]
		Normalizing factor for the DISTNORM image [‡]	Normalizing factor for the Vo12 image [‡]
		Normalizing factor for the 2D sky map image [‡]	Normalizing factor for the 2D sky map image [‡]
		Normalized posterior mean distance	Normalized posterior mean distance
			Normalized \log BCI
			Normalized \log BSN

[†]For Cabero et al. (2020) and the Baseline model, the elements are used to indicate whether the LIGO Hanford, LIGO Livingston, and Virgo detectors were operating at the time of a GW candidate. For the Fine-tuned model, however, the elements are used to indicate the detectors with $\text{SNR} \geq 4.5$. Future updates of GWSkyNet will extend the model to incorporate KAGRA (Akutsu et al. 2020; Aso et al. 2013) and LIGO India (Abbott et al. 2018; Iyer et al. 2011).

[‡]All normalizing factors are also normalized by the maximum of the corresponding value from the entire training data set.

Table 1. The inputs for the GWSkyNet model. The first column indicates whether the corresponding input feature is images or numerical data. The second and third columns show the inputs to the GWSkyNet model published in Cabero et al. (2020) and those for the updated GWSkyNet model presented in this paper respectively. The numbers in the brackets indicate the image dimension in pixels.

of the data it has been trained on may result in sub-optimal performances. As different noise sources may contribute differently to the noise budget across observing runs, data from separate observing runs may show distinctive features and characteristics. For example, glitches may have diverse morphology across observing runs because instrument configurations have changed. Similar glitches may also occur at different rates.

To ensure the classifier learns a generalization that is representative of the GW candidates expected in O4, we retrain and fine-tune the GWSkyNet model. This section will focus on retraining and the next section on fine-tuning. To retrain, we first compile training samples using O3 data from the Gravitational Wave Open Science Centre.⁴ Since GWSkyNet is a signal versus noise classifier, we generate data of these two classes. For both classes, we employ a procedure similar to that presented in Cabero et al. (2020). In particular, we simulate a population of GWs from mergers of binary black holes (BBHs), neutron star black holes (NSBHs) and BNSs using gravitational waveform models available in the LALSuite package (LIGO Scientific Collaboration 2018). To allow the simulated data to be as realistic and representative of those expected in low latency as possible, we add the simulated GWs to Gaussian noise

colored by the power spectral densities associated with the GW alerts released during O3 from GraceDB. The simulated signals are distributed equally among these different representative power spectral densities.

A population of noise events from known glitches in O3 is also identified for training using a GW trigger list from the fourth Open Gravitational-wave Catalog (Nitz et al. 2023) and a collection of glitches from the Gravity Spy classifier. Gravity Spy is a scientific initiative that combines human expertise, machine learning and citizen scientist with the aim of classifying detector noise transients based on their morphologies (Zevin et al. 2017; Bahaadini et al. 2018; Coughlin et al. 2019; Zevin et al. 2023).

A signal-to-noise ratio (SNR) requirement is then implemented to select the candidates that are observed in at least two detectors with an SNR of no less than 4.5 and a network SNR, given by the quadrature sum of the individual SNR, of greater than or equal to 7.0. In total, ~ 17400 event candidates were generated for the training of the GWSkyNet model, with approximately 8700 for each class. In particular, the ~ 8700 remaining noise events include all types of glitches found in Gravity Spy. An example noise candidate is shown in Figure 2. A gravitational waveform of a coincident 4-OGC trigger is also shown. A model trained on this data set will be able to learn features and patterns in GW candidates broadly consistent with those expected in low-latency

⁴ <https://gwosc.org/>

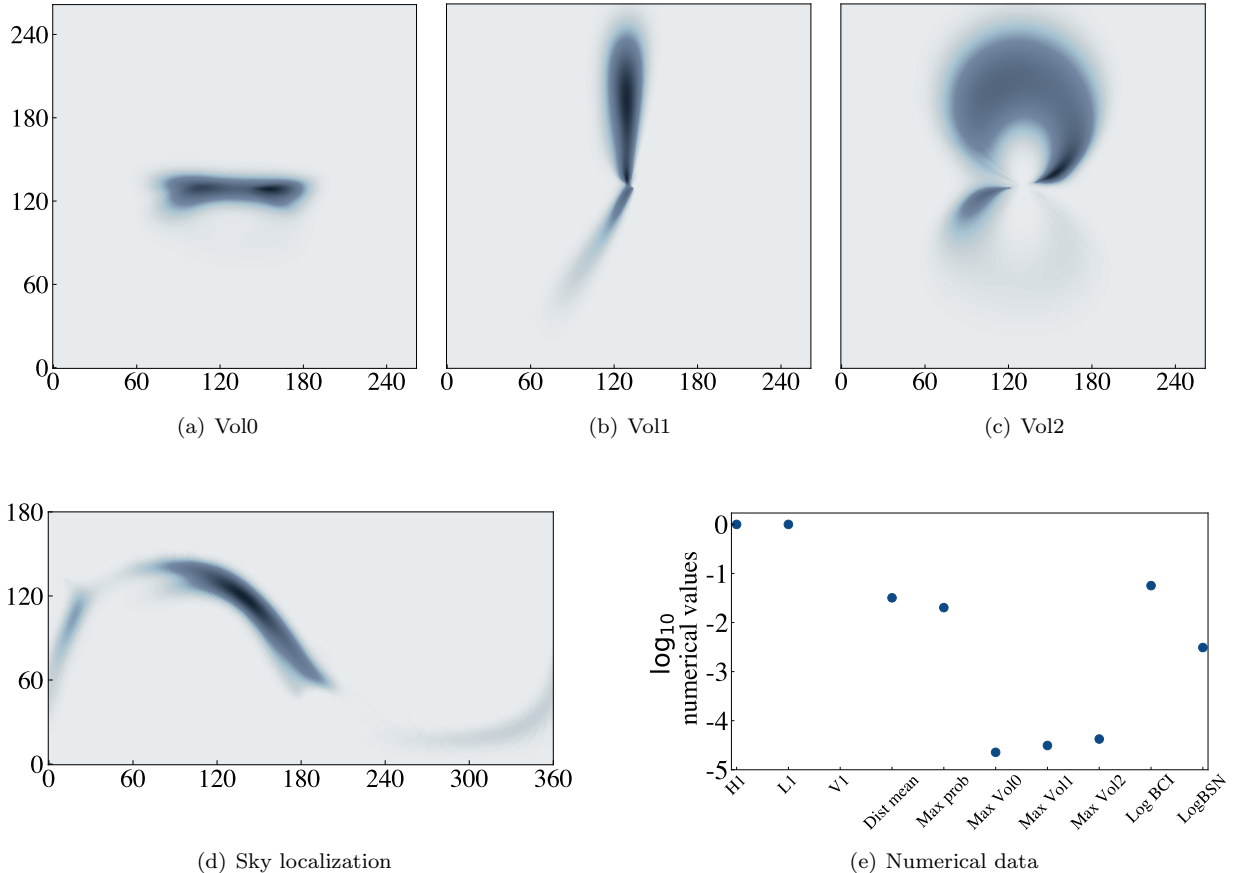


Figure 1. Input images and numerical data extracted from the FITS file of S191120at for *GWSkyNet*. The top row shows the 3 volume reconstruction images of the event. The left plot in the bottom row shows a 2D projection of the sky localization. For the images, the x and y axes indicate the pixels. The bottom right plot shows the numerical data extracted from the associated FITS file that are also used as inputs.

searches, allowing to establish a baseline performance. For the rest of the paper, this training data set will be referred to as the Baseline data set and the model as the Baseline model.

2.3. Fine-tuning

To evaluate the performance of the LVK low-latency infrastructure and its readiness for O4, the LVK collaboration has organized a MDC campaign as part of the preparation for O4. The MDC consisted of 40 days of detector data collected by LIGO and Virgo from 5 Jan. 2020 15:59:42 to 14 Feb. 2020 15:59:42 UTC. A total of 5×10^4 simulated GW signals from mergers of BNSs, NSBHs and BBHs with a minimum network SNR of 4 were added to the data at a rate of one per ~ 40 seconds. The data were then replayed and analyzed by search pipelines in low-latency configurations as if the data were just collected. Once the replay of the 40 days of data is completed, a new cycle will ensue. Details regarding the distributions of the simulated GW signals can be found in [Chaudhary & Toivo-](#)

[nen et al. \(2023\)](#). The MDC campaign allows search pipelines to refine their configurations for low-latency searches such as the construction of template banks, the ranking statistics and the estimation of candidate significance ([Ewing et al. 2024a](#)), leading to more accurate and sensitive search pipelines.

However, such evolving configurations could result in identifying a population of GW candidates that differs from that represented by the Baseline data set. In addition, the false alarm rate (FAR) estimate of GW candidates by search pipelines in low-latency is a key statistic in determining whether the candidates will be released as public alerts,¹ while such information is generally not available for the Baseline data set.

To overcome the weaknesses, we use the GW candidates identified in a MDC cycle of the MDC campaign by search pipelines to fine-tune the Baseline model to GW candidates generated by low-latency searches. Fine-tuning is a common technique in transfer learning. During fine-tuning, the weights of a pre-trained model are fine-tuned on a target data set (see [Pan &](#)

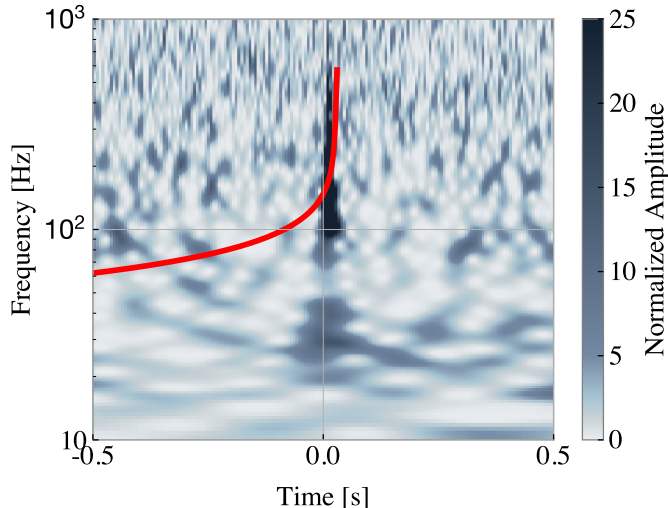


Figure 2. Time-frequency representation of a blip glitch at LIGO Livingston from O3. The red curve represents the GW template that triggered the 4-OGC search. This template corresponds to a NSBH merger with component masses of $m_1 = 23M_\odot$ and $m_2 = 2M_\odot$. The network SNR of the candidate by the search is 7.6.

Yang (2009)). As only the event candidates with a FAR ≤ 2 per day will be released as public alerts in O4,¹ we first select all the noise event candidates with FAR ≤ 2 per day. The SNR requirement defined in section 2.2 is applied, leaving approximately 300 candidates. An equal number of simulated GW events are then selected randomly. We then augment the data by shifting the observing time randomly at which the GW candidates were observed, changing the right ascension and declination of the sky localizations. This results in a data set of ~ 12000 samples. This approaches the maximum number achievable with augmentation by changing the observing times, as shifting the observing time by multiples of approximately 24 hours would lead to an identical sky localization. We will refer to this data set as the Fine-tuned data set. Since the number of distinct GW candidates in this data set is significantly lower than that in the Baseline data set, allowing all the layers of the Baseline model to be trainable may result in the model forgetting the generalization learned from the Baseline data set and overfitting the Fine-tuned data set. We therefore freeze the majority of the layers of the Baseline models and only allow the three dense layers in the two convolutional branches and the final layer to be trainable (see Figure 3 in Cabero et al. (2020)). Also, we find that by adopting a more refined physical definition for the input binary array for detectors to indicate detectors with a SNR of 4.5 or greater (see Table 1), a better performance can be achieved. This is because data

from all three detectors may be used to produce GW candidate localization even if the candidate has negligible SNR in one detector. The resulting model is referred to as the Fine-tuned model. Both the Baseline model and the Fine-tuned model are then applied to a new and more recent cycle of the MDC campaign to evaluate the performance, which will be referred to as the test MDC cycle. The results are shown in the next section.

3. PERFORMANCE

During the test MDC cycle, 4016 event candidates were identified by at least one LVK CBC search pipeline with a FAR ≤ 2 per day that met the SNR requirement specified in section 2.2. Of these 4016 candidates, 3913 were simulated GW events and 96 were noise transients. The remaining 7 were real GW events reported in Abbott et al. (2021c). We quantify the performance of both the Baseline model and the Fine-tuned model on these 4016 events with false alarm probability (FAP) and false negative probability (FNP). The FAP is an empirical measure of the fraction of noise event candidates at or above a candidate’s **GWSkyNet** score. Similarly, the FNP is an empirical measure of the fraction of simulated GW candidates at or below a candidate’s **GWSkyNet** score. In the upper left panel of Figure 3 we show the FAP and FNP as a function of **GWSkyNet** score.

To present the performance of **GWSkyNet** from another perspective, we also construct the receiver operator characteristic (ROC) curve in the upper right panel. The ROC curve is one of the most commonly used and convenient ways to determine the classification performance of a signal detection algorithm. It shows the performance of a classifying model by defining the probability of detection, which is the fraction of simulated GW candidates correctly identified, as a function of the FAP. The ROC curve is obtained by computing the FAP and probability of detection at different values of **GWSkyNet** score. For a given FAP, a model with a higher probability of detection is considered more capable than a model with a lower probability of detection. At a FAP of 20%, the Fine-tuned model achieves a probability of detection of 92.5% while the Baseline model obtains a probability of detection of 68.3% clearly suggesting the necessity of fining-tuning **GWSkyNet** to the configurations of search pipelines. However, we note that the improvement in the performance is largely attributed to an increase in probability of detection at FAP $\lesssim 0.35$ for three-detector events. As shown in Figure 3(b), for event candidates identified by networks of two detectors, the Baseline and Fine-tuned models have comparable performance. For example, at a FAP of 20%, the true alarm probabilities (TAPs) for the Base-

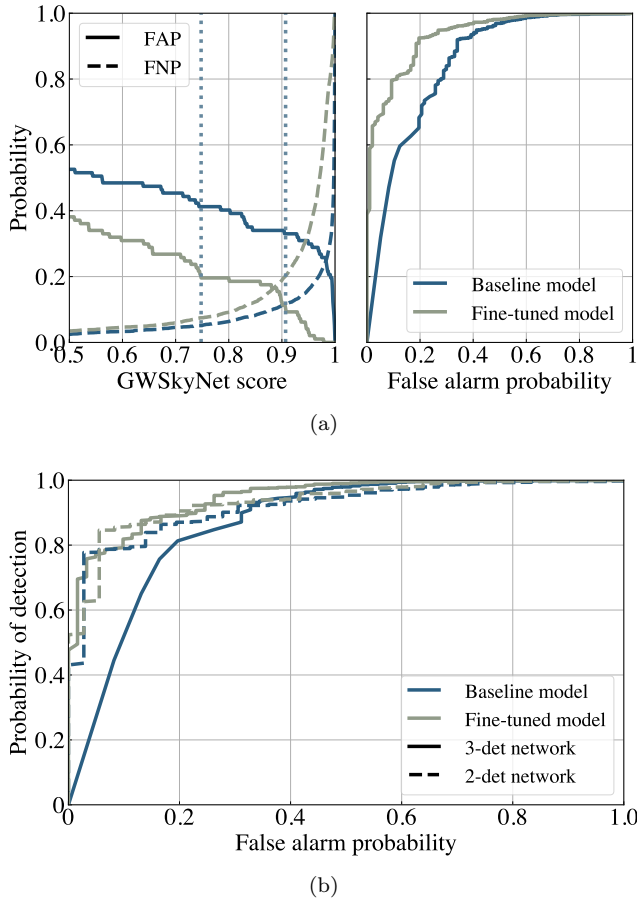


Figure 3. The performance of both the Baseline and Fine-tuned model on the LVK-led MDC (the test MDC cycle). The upper left panel shows the FAP and FNP as a function of the *GWSkyNet* score, while the upper right panel shows the probability of detection as a function of FAP. The dotted lines in the upper left panel indicate the FAPs and FNPs at two different *GWSkyNet* scores corresponding to two different use cases with the Fine-tuned model described in section 4. The upper panels are for all events that met the SNR requirement specified in section 2.2. The bottom panel shows the performances of the Baseline and Fine-tuned models for events identified by two-detector networks and three-detector networks respectively.

line and the Fine-tuned models are 91% and 88% for two detector events, while the TAPs are 90% and 81% for three-detector events. By adjusting the *GWSkyNet* score threshold, one can achieve a desired probability of detection, while keeping an acceptable FAP based on one’s risk tolerance. The confusion matrices in Figure 4 demonstrate the performance achieved by thresholding on a *GWSkyNet* score so that FAP and FNP are balanced. We expect O4 will first operate with a two-detector configuration and transition to a three-detector configuration with Virgo joining in early 2024.¹ This will coincide with the expected implementation of the Baseline

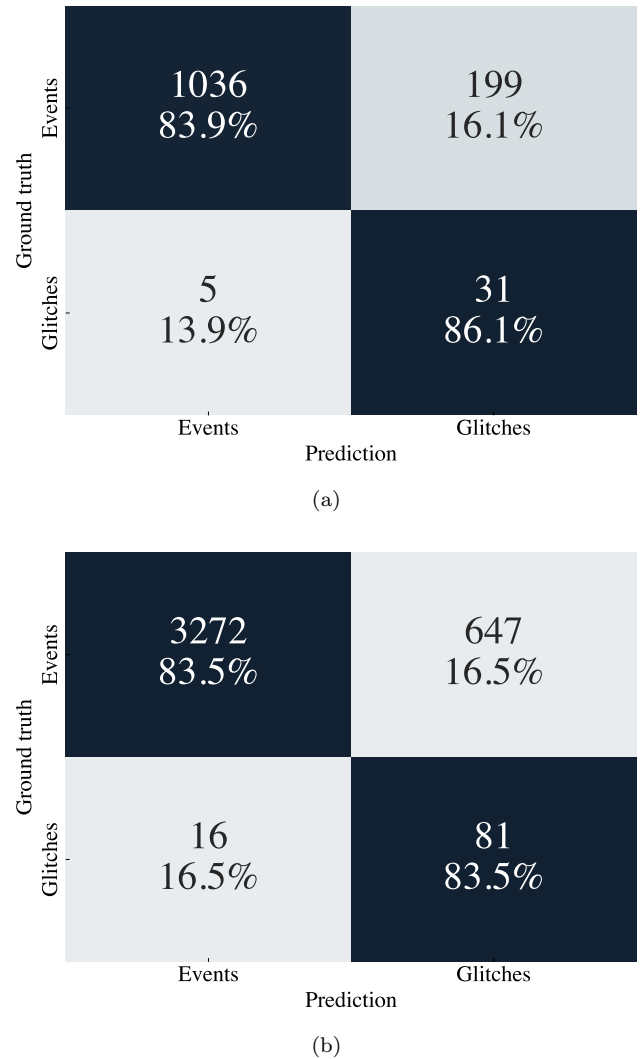


Figure 4. Confusion matrices depicting the performances of the Baseline and Fine-tuned models on events identified during the test MDC cycle. The upper panel shows the Baseline model’s performance for two-detector events, and the lower shows the Fine-tuned model’s performance for both two-detector and three-detector events. The confusion matrices are generated using a *GWSkyNet* score threshold that balances the FAP and FNP. For the Baseline model, this threshold is 0.785, while it is 0.885 for the Fine-tuned model.

and Fine-tuned models (see section 4). Therefore, for the Baseline model, we show the performance for two-detector events at a *GWSkyNet* score threshold of 0.785, while for the Fine-tuned model, the performance is for all events at a *GWSkyNet* score threshold of 0.885. However, the small number of glitches available in the test MDC cycle suggests the performance of the models may deviate in practice. The results can be taken only as reference.

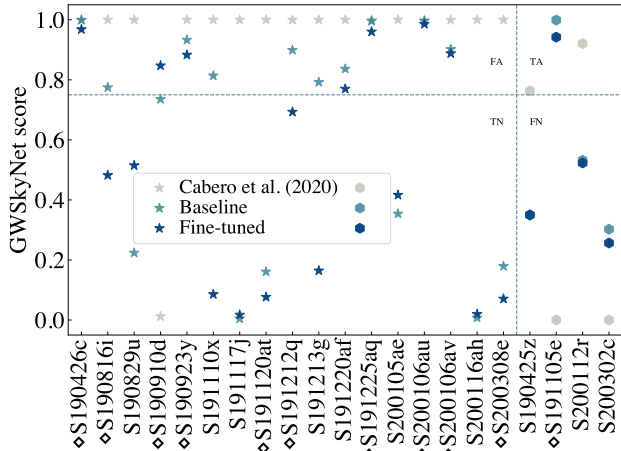


Figure 5. A scatter plot showing the misidentifications of O3 alerts by the GWSkyNet models (Baseline model, Fine-tuned model and Cabero et al. (2020)). The horizontal axis shows the IDs of the alerts that are misclassified by at least one model. The symbol \diamond next to the IDs indicates whether the SNR of the alerts would have met the SNR requirement defined in section 2.2 and thus whether would have been analyzed by GWSkyNet. The vertical axis is the GWSkyNet score. Stars indicate glitches and hexagons indicate GW signals according to Abbott et al. (2021c); Abbott et al. (2024). The GWSkyNet score threshold (0.75) used to determine the misidentifications is indicated by the horizontal dashed line. The vertical dashed line separate glitches and GW events.

In addition, to allow for a direct comparison between the model in Cabero et al. (2020) and the models in this paper, we apply both the Baseline and Fine-tuned model to the 77 CBC alerts published in O3. To ensure this is a representative test, we use the sky localization information produced by BAYESTAR that was immediately available at the time of the alerts. Of the 77 alerts, 64 and 67 are correctly identified by the Baseline and Fine-tuned models respectively (assuming a GWSkyNet score threshold of 0.75 (see section 4) and according to Abbott et al. (2021c); Abbott et al. (2024)), which is 5 and 8 more correct identifications or $\sim 6\%$ and $\sim 10\%$ more accurate than the original GWSkyNet model, showing improvement over an already well performing model. Figure 5 shows the misclassifications by the models. The misclassifications are also presented in a tabular format in Table 3 in Appendix. As a reference, we also provide the GWSkyNet scores by the Baseline model (see section 4) for O4 public alerts in Table 2. For 95% of the O4 public alerts analyzed by GWSkyNet, the time between the release of the public alerts and the completion of the analysis by GWSkyNet is ≤ 66 seconds.

3.1. Interpretation when signals and glitches overlap

Due to the high glitch rate of O3 (Abbott et al. 2021a,c), a significant number of simulated GW signals in the MDC happened to be added at a time close to the occurrence of a glitch. The presence of a nearby or overlapping glitch may impact the estimates of the source parameters and the localization of the event candidate (Macas et al. 2022; Huber & Davis 2022; Pankow et al. 2018; Powell 2018). An example is shown in Figure 6. A simulated GW signal visible in LIGO Livingston is added at a time coincident with a glitch in LIGO Hanford. Two sky localization maps corresponding to the simulated GW signals are shown in Figure 7. The upper panel shows the sky localization by LIGO Hanford, LIGO Livingston and Virgo, while the lower panel shows that by LIGO Livingston and Virgo only. The true location of the event is not consistent with the 90% credible region in the upper panel because of the presence of the glitch. The GWSkyNet score by the Fine-tuned model for the upper and lower sky localization is 2.0×10^{-13} and 0.96 respectively. A low GWSkyNet score for an initial sky localization of a GW candidate similar to the upper panel may be mistakenly assumed to mean the absence of a GW signal in the data. Even if a more accurate sky map for the same event later becomes available, follow-up observations may still be discouraged if the sky map is produced with lower SNR such that it is not evaluated by GWSkyNet. Conversely, a high GWSkyNet score (e.g., above 0.90) for a candidate where the source is located outside the 90% credible region may lead to an assumption that the localization is accurate such that the source is located in the 90% credible region. As stated above, the GWSkyNet score should be considered to mean the GWSkyNet model’s confidence that the localization information is both internally consistent and aligns with that of a GW signal. Careful interpretation is necessary.

4. IMPLEMENTATION

GWSkyNet is an algorithm that analyzes the end products from search pipelines (i.e., the sky localization information encoded in FITS files and the associated metadata). This allows GWSkyNet to evaluate GW events from a perspective that is different from standard search pipelines, which usually analyze GW detector time series data. GWSkyNet thus supplies a complementary metric for the interpretation of the origin of event candidates that can be used to reduce false positives attributed to detector noise and consistently compared across different search pipelines. The use of GWSkyNet also enables the identification of the sky maps for a GW candidate more consistent with a GW signal.

Alert ID	GWSkyNet score	Retracted
S230518h	0.995	False
S230520ae	0.995	False
S230601bf	0.931	False
S230605o	0.986	False
S230606d	0.937	False
S230608as	0.981	False
S230609u	0.978	False
S230622ba	0.611	True
S230624av	0.970	False
S230627c	0.987	False
S230628ax	0.993	False
S230630am	0.991	False
S230630bq	0.933	False
S230702an	0.967	False
S230704f	0.863	False
S230706ah	0.978	False
S230707ai	0.962	False
S230708t	0.950	False
S230708z	0.981	False
S230708cf	0.934	False
S230709bi	0.970	False
S230715bw	0.000	True
S230723ac	0.948	False
S230729z	0.987	False
S230731an	0.992	False
S230805x	0.972	False
S230806ak	0.975	False
S230807f	0.921	False
S230811n	0.994	False
S230814r	0.992	False
S230819ax	0.988	False
S230820bq	0.695	False
S230824r	0.992	False
S230825k	0.935	False
S230831e	0.989	False
S230904n	0.989	False
S230914ak	0.997	False
S230919bj	0.999	False
S230920al	0.988	False
S230922g	0.895	False
S230922q	0.997	False
S230924an	0.997	False
S230927l	0.995	False
S230927be	0.997	False
S230928cb	0.999	False
S230930al	0.965	False
S231001aq	0.942	False
S231005j	0.999	False
S231005ah	0.967	False

Table 2. The GWSkyNet scores by the Baseline model for the O4 GW candidates that have been published as of this writing, using the sky localization information that was immediately available at the time of the alerts. The list is not comprehensive as only the alerts where the SNR meet the SNR requirements defined in section 2.2 were analyzed with GWSkyNet. Assuming a GWSkyNet score threshold of 0.75 (see section 4), GWSkyNet has correctly classified the retracted events (S230622ba and S230715bw).

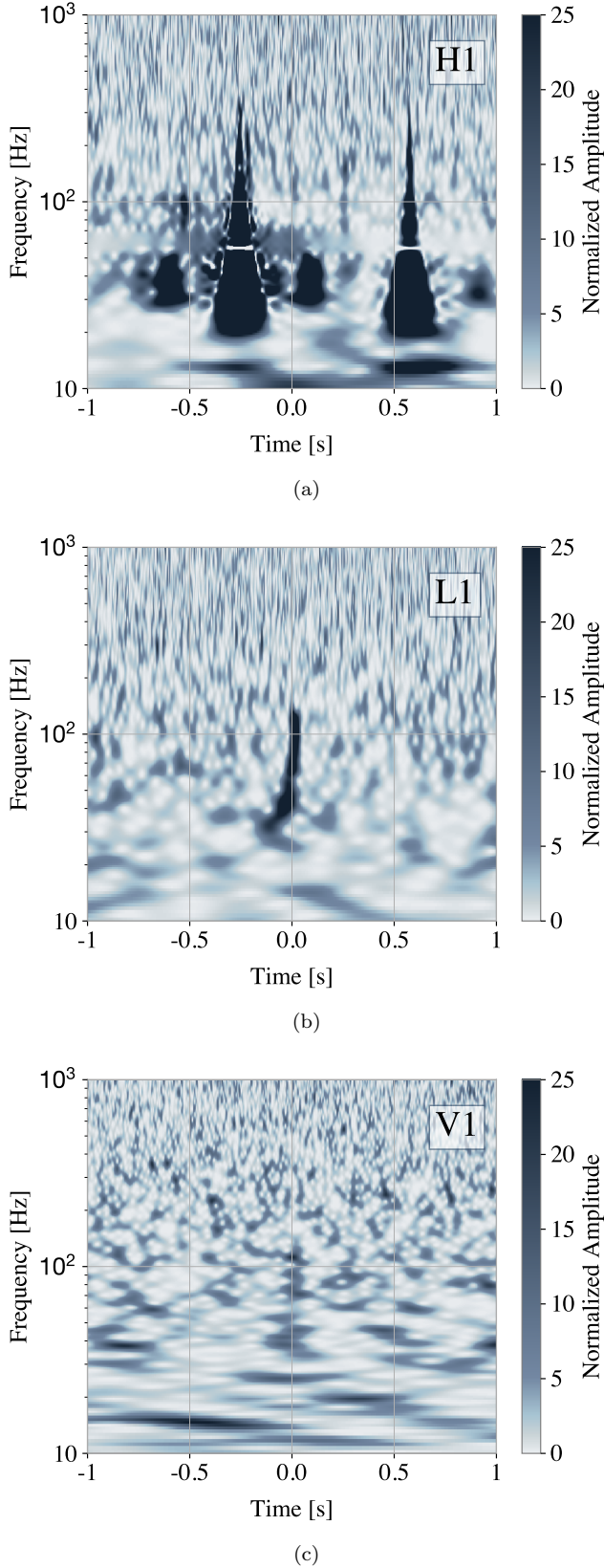


Figure 6. Time-frequency representations of a simulated GW candidate in the LIGO and Virgo detectors. The merger time of the simulated GW is at 0s. The signal is visible in the spectrogram for LIGO Livingston (b). However, a loud glitch is coincident with the GW signal and dominates the spectrogram for LIGO Hanford (a).

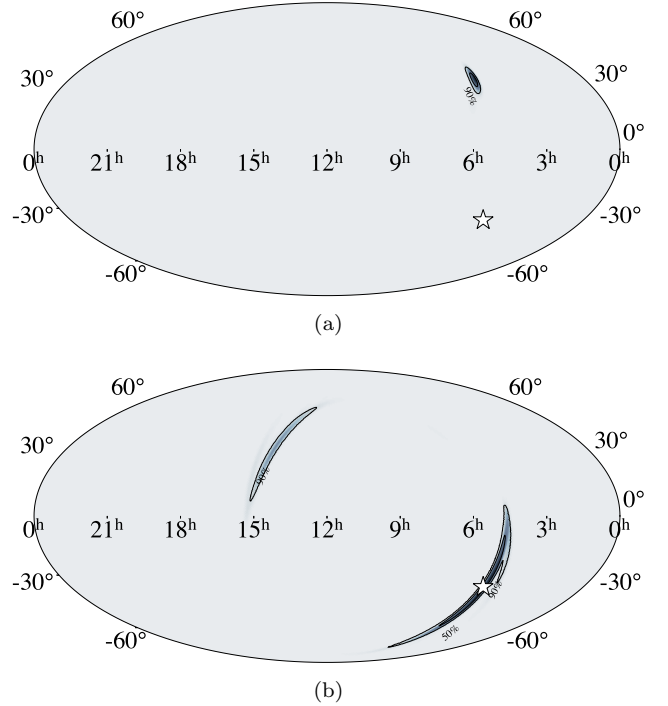


Figure 7. The sky localization of the simulated GW event shown in Figure 6 by BAYESTAR. The upper panel shows the localization by LIGO Hanford, LIGO Livingston and Virgo, while the lower shows that by LIGO Livingston and Virgo. The true location of the event is marked by a star in both sky maps. In this example, the true location is not consistent with the 90% credible region in the upper panel.

EM counterparts of GW events may fade quickly after merger and early epoch observations of EM counterparts are critical in constraining the properties of GW sources (Abbott et al. 2017b; Drout et al. 2017; Coulter et al. 2017; Smartt et al. 2017; Goldstein et al. 2017; Savchenko et al. 2017; Abbott et al. 2017b; Abbott et al. 2017a). For instance, optical and ultraviolet observation of the kilonova associated with a BNS merger in the first few hours after merger is necessary for breaking emission model degeneracy (Arcavi 2018). For this purpose, *GWSkyNet* is most useful if implemented as an automatic low-latency pipeline that evaluates the origin of GW alerts. To this end, we integrated *GWSkyNet* with the Baseline model into the LVK’s low-latency infrastructure (*GWcElery*).⁵ The Fine-tuned model will be implemented in our next update. This will coincide with Virgo joining O4 when event candidates may trigger three detectors simultaneously. The integration allows *GWSkyNet* to listen and react to public GW alerts in real time. *GWSkyNet* is currently operating for O4.

⁵ <https://rtd.lgw.org/projects/gwcelery/en/latest/index.html>

For a GW public alert identified with a network SNR of ≥ 7.0 and an SNR of ≥ 4.5 in at least two detectors, a **GWSkyNet** score, and the empirical measurements of FAP and FNP given by Figure 3(a) are provided on GraceDB. These three quantities allow astronomers and other GW analyses to screen noise based on their tolerance of false positives and the amount of resources that they can spend. As indicated in Figure 3(a), using the Fine-tuned model as an example, for an astronomer with ample telescope time who seeks to compile a list of promising candidates as large as possible, a **GWSkyNet** score threshold of 0.75 can be used to reject 80% noise and capture 93% astrophysical signals. On the other hand, if the astronomer is hoping to follow up on the GW candidates most likely to be of astrophysical origin, a **GWSkyNet** score threshold of 0.91 can be used to reject 90% noise and catch 80% of astrophysical signals. However, we emphasize the small number of glitches in the test MDC cycle suggests that these statistics can only be used as references and performance in practice may deviate. In the future, as **GWSkyNet** continues to operate for O4 and accumulates sufficient statistics, the FAP and FNP will be more reliable and can be incorporated into the **GWSkyNet** score to provide a calibrated probability that a GW candidate is of astrophysical origin.

5. SUMMARY

GWSkyNet is a machine learning classifier developed to facilitate EM follow-up observations of GW candidates. The classifier leverages the sky localization information of LVK event candidates encoded in the FITS file and the metadata associated with GW candidates. The use of sky localization information instead of detector time series data allows a unique evaluation of event candidates. It also provides a metric that can be compared directly and interpreted consistently across all search pipelines.

We reviewed and improved the architecture of the **GWSkyNet** model and the inputs to allow a more effective normalization of the data and better generalization by the classifier. Our results for the LVK MDC campaign show promising accuracy. In particular, using a **GWSkyNet** score threshold of 0.75, the Fine-tuned model allows the rejection of more than 80% noise while capturing more than 93% astrophysical signals. Additionally, the Fine-tuned model correctly identify 67 public alerts during O3 assuming a **GWSkyNet** score threshold of 0.75, 8 more than the original **GWSkyNet** model.

We also show that for signals where a glitch is close in time or overlapping, resulting in a noise-influenced sky localization, careful interpretation of the **GWSkyNet**

score is encouraged. We emphasize the **GWSkyNet** score should be interpreted as the **GWSkyNet** model’s confidence that the input localization information is consistent internally and with a GW signal.

To facilitate EM follow-up observations of GW events, we integrated **GWSkyNet** into LVK’s low-latency infrastructure that responds to GW candidates in real time in O4. For each event candidate, three quantities are provided and made available on GraceDB: **GWSkyNet** score and the empirical measurement of FAP and FNP. The use of these quantities allows a trade-off between rejecting noise and capturing true astrophysical signals.

ACKNOWLEDGMENT

We are thankful to the following individuals for their valuable contributions to the development and success of **GWSkyNet**, without which **GWSkyNet** would not have been possible. We wish to thank Maria Drout, Aaron Tohuvavohu, Derek Davis, Brandon Piotrkowski, Deep Chatterjee, Leo Singer, Erik Katsavounidis, Patrick Brockill, Reed Essick, Beverly Berger, Alan Knee and Jonah Kanner for their valuable feedback and suggestions, which helped us refine **GWSkyNet** as a pipeline. J.M. acknowledges funding from the Natural Sciences and Engineering Research Council of Canada (NSERC). A.M. acknowledges support from the NSF (1640818, AST-1815034). A.M. and J.M. also acknowledge support from IUSSTF (JC-001/2017). D.H. and J.M. acknowledge support from the Canada Research Chairs (CRC) program, the NSERC Discovery Grant program, and the Canadian Institute for Advanced Research (CIFAR). The authors highlight support for this project from the Canadian Tri-Agency New Frontiers in Research Fund – Exploration program. M. W. Coughlin acknowledges support from the National Science Foundation with grant numbers PHY-2347628 and PHY-2117997. N.R. acknowledges funding support from the Trottier Space Institute at McGill and the Walter C. Sumner Memorial Fellowship. This material is based upon work supported by NSF’s LIGO Laboratory which is a major facility fully funded by the National Science Foundation.

Alert ID	Cabero et al. (2020)	Baseline	Fine-tuned	True label	SNR criteria met
S190425z ^{†*}	0.76	0.35	0.35	Real	False
S190426c ^{†‡*}	1.00	1.00	0.97	Glitch	True
S190816i ^{†‡}	1.00	0.77	0.48	Glitch	True
S190829u [†]	1.00	0.22	0.51	Glitch	False
S190910d [*]	0.01	0.74	0.85	Glitch	True
S190923y ^{†‡*}	1.00	0.93	0.88	Glitch	True
S191105e [†]	0.00	1.00	0.94	Real	True
S191110x ^{†‡}	1.00	0.81	0.09	Glitch	False
S191117j [†]	1.00	0.00	0.02	Glitch	False
S191120at [†]	1.00	0.16	0.08	Glitch	True
S191212q ^{†‡}	1.00	0.90	0.69	Glitch	True
S191213g ^{†‡}	1.00	0.79	0.16	Glitch	False
S191220af ^{†‡*}	1.00	0.84	0.77	Glitch	False
S191225aq ^{†‡*}	1.00	1.00	0.96	Glitch	True
S200105ae [†]	1.00	0.35	0.42	Glitch	False
S200106au ^{†‡*}	1.00	1.00	0.99	Glitch	True
S200106av ^{†‡*}	1.00	0.90	0.89	Glitch	True
S200112r ^{†*}	0.92	0.53	0.52	Real	False
S200116ah [†]	1.00	0.00	0.02	Glitch	False
S200302c ^{†‡*}	0.00	0.30	0.26	Real	False
S200308e [†]	1.00	0.18	0.07	Glitch	True

Table 3. Misidentifications of O3 public alerts by the three **GWSkyNet** models. The first column displays the IDs of the alerts. The superscripts †, ‡ and * indicate misidentifications by Cabero et al. (2020), the Baseline model and the Fine-tuned model respectively. Columns 2-4 show the **GWSkyNet** scores for the alerts by the specific models. The true labels of the alerts are based on Abbott et al. (2021c); Abbott et al. (2024). The last column indicates whether the SNR of the alerts would have met the SNR requirement defined in this paper and thus whether would have been analyzed by **GWSkyNet**.

APPENDIX

REFERENCES

- Abbott, B. P., Abbott, R., Abbott, T. D., et al. 2017a, *PhRvL*, 119, 161101, doi: [10.1103/PhysRevLett.119.161101](https://doi.org/10.1103/PhysRevLett.119.161101)
- . 2017b, *ApJL*, 848, L12, doi: [10.3847/2041-8213/aa91c9](https://doi.org/10.3847/2041-8213/aa91c9)
- Abbott, B. P., et al. 2017a, *Astrophys. J. Lett.*, 848, L13, doi: [10.3847/2041-8213/aa920c](https://doi.org/10.3847/2041-8213/aa920c)
- . 2017b, *Nature*, 551, 85, doi: [10.1038/nature24471](https://doi.org/10.1038/nature24471)
- . 2018, *Living Rev. Rel.*, 21, 3, doi: [10.1007/s41114-020-00026-9](https://doi.org/10.1007/s41114-020-00026-9)
- Abbott, B. P., Abbott, R., Abbott, T. D., et al. 2019, *Physical Review X*, 9, 031040, doi: [10.1103/PhysRevX.9.031040](https://doi.org/10.1103/PhysRevX.9.031040)
- Abbott, R., Abbott, T. D., Abraham, S., et al. 2021a, *Physical Review X*, 11, 021053, doi: [10.1103/PhysRevX.11.021053](https://doi.org/10.1103/PhysRevX.11.021053)
- Abbott, R., et al. 2024, *Phys. Rev. D*, 109, 022001, doi: [10.1103/PhysRevD.109.022001](https://doi.org/10.1103/PhysRevD.109.022001)
- Abbott, T. C., Buffaz, E., Vieira, N., et al. 2021b, arXiv e-prints, arXiv:2111.04015, <https://arxiv.org/abs/2111.04015>
- Abbott, T. D., Acernese, F., Ackley, K., et al. 2021c, arXiv e-prints, arXiv:2111.03606, <https://arxiv.org/abs/2111.03606>
- Adams, T., Buskulic, D., Germain, V., et al. 2016, *Classical and Quantum Gravity*, 33, 175012
- Akutsu, T., Ando, M., Arai, K., et al. 2020, *Progress of Theoretical and Experimental Physics*, 2021, 05A101, doi: [10.1093/ptep/ptaa125](https://doi.org/10.1093/ptep/ptaa125)

- Annala, E., Gorda, T., Kurkela, A., & Vuorinen, A. 2018, *Phys. Rev. Lett.*, 120, 172703, doi: [10.1103/PhysRevLett.120.172703](https://doi.org/10.1103/PhysRevLett.120.172703)
- Antier, S., Agayeva, S., Almualla, M., et al. 2020, *Monthly Notices of the Royal Astronomical Society*, 497, 5518, doi: [10.1093/mnras/staa1846](https://doi.org/10.1093/mnras/staa1846)
- Arcavi, I. 2018, *Astrophys. J. Lett.*, 855, L23, doi: [10.3847/2041-8213/aab267](https://doi.org/10.3847/2041-8213/aab267)
- Aso, Y., Michimura, Y., Somiya, K., et al. 2013, *Phys. Rev. D*, 88, 043007, doi: [10.1103/PhysRevD.88.043007](https://doi.org/10.1103/PhysRevD.88.043007)
- Aubin, F., et al. 2021a, *Class. Quant. Grav.*, 38, 095004, doi: [10.1088/1361-6382/abe913](https://doi.org/10.1088/1361-6382/abe913)
- Aubin, F., Brighenti, F., Chierici, R., et al. 2021b, *Classical and Quantum Gravity*, 38, 095004, doi: [10.1088/1361-6382/abe913](https://doi.org/10.1088/1361-6382/abe913)
- Bahaadini, S., Noroozi, V., Rohani, N., et al. 2018, *Information Sciences*, 444, 172
- Bauswein, A., Just, O., Janka, H.-T., & Stergioulas, N. 2017, *The Astrophysical Journal Letters*, 850, L34, doi: [10.3847/2041-8213/aa9994](https://doi.org/10.3847/2041-8213/aa9994)
- Cabero, M., Mahabal, A., & McIver, J. 2020, *ApJL*, 904, L9, doi: [10.3847/2041-8213/abc5b5](https://doi.org/10.3847/2041-8213/abc5b5)
- Chan, M. L., et al. 2020, *Phys. Rev. D*, 102, 043022, doi: [10.1103/PhysRevD.102.043022](https://doi.org/10.1103/PhysRevD.102.043022)
- Chatterjee, C., Wen, L., Beveridge, D., Diakogiannis, F., & Vinsen, K. 2022, arXiv preprint arXiv:2207.14522
- Chaudhary, S. S., Toivonen, A., et al. 2023. <https://arxiv.org/abs/2308.04545>
- Chornock, R., Berger, E., Kasen, D., et al. 2017, *The Astrophysical Journal Letters*, 848, L19
- Chu, Q., et al. 2022a, *Phys. Rev. D*, 105, 024023, doi: [10.1103/PhysRevD.105.024023](https://doi.org/10.1103/PhysRevD.105.024023)
- Chu, Q., Kovalam, M., Wen, L., et al. 2022b, *Phys. Rev. D*, 105, 024023, doi: [10.1103/PhysRevD.105.024023](https://doi.org/10.1103/PhysRevD.105.024023)
- Coughlin, M. W., Dietrich, T., Margalit, B., & Metzger, B. D. 2019a, *Monthly Notices of the Royal Astronomical Society: Letters*, 489, L91, doi: [10.1093/mnrasl/slz133](https://doi.org/10.1093/mnrasl/slz133)
- Coughlin, M. W., Dietrich, T., Doctor, Z., et al. 2018, *Monthly Notices of the Royal Astronomical Society*, 480, 3871, doi: [10.1093/mnras/sty2174](https://doi.org/10.1093/mnras/sty2174)
- Coughlin, M. W., Dietrich, T., Antier, S., et al. 2019b, *Monthly Notices of the Royal Astronomical Society*, 492, 863, doi: [10.1093/mnras/stz3457](https://doi.org/10.1093/mnras/stz3457)
- Coughlin, M. W., Dietrich, T., Heinzel, J., et al. 2020a, *Phys. Rev. Res.*, 2, 022006, doi: [10.1103/PhysRevResearch.2.022006](https://doi.org/10.1103/PhysRevResearch.2.022006)
- Coughlin, M. W., Antier, S., Dietrich, T., et al. 2020b, *Nature communications*, 11, 4129
- Coughlin, S., Bahaadini, S., Rohani, N., et al. 2019, *PhRvD*, 99, 082002, doi: [10.1103/PhysRevD.99.082002](https://doi.org/10.1103/PhysRevD.99.082002)
- Coulter, D. A., Foley, R. J., Kilpatrick, C. D., et al. 2017, *Science*, 358, 1556, doi: [10.1126/science.aap9811](https://doi.org/10.1126/science.aap9811)
- Cowperthwaite, P. S., Berger, E., Villar, V., et al. 2017, *The Astrophysical Journal Letters*, 848, L17
- Cuoco, E., Powell, J., Cavaglià, M., et al. 2020, *Machine Learning: Science and Technology*, 2, 011002, doi: [10.1088/2632-2153/abb93a](https://doi.org/10.1088/2632-2153/abb93a)
- Dal Canton, T., Nitz, A. H., Gadre, B., et al. 2021, *The Astrophysical Journal*, 923, 254
- Dietrich, T., Coughlin, M. W., Pang, P. T. H., et al. 2020, *Science*, 370, 1450, doi: [10.1126/science.abb4317](https://doi.org/10.1126/science.abb4317)
- Drout, M. R., Piro, A. L., Shappee, B. J., et al. 2017, *Science*, 358, 1570, doi: [10.1126/science.aaq0049](https://doi.org/10.1126/science.aaq0049)
- Ewing, B., Huxford, R., Singh, D., et al. 2024a, *Phys. Rev. D*, 109, 042008, doi: [10.1103/PhysRevD.109.042008](https://doi.org/10.1103/PhysRevD.109.042008)
- . 2024b, *Phys. Rev. D*, 109, 042008, doi: [10.1103/PhysRevD.109.042008](https://doi.org/10.1103/PhysRevD.109.042008)
- Gabbard, H., et al. 2018, *Phys. Rev. Lett.*, 120, 141103, doi: [10.1103/PhysRevLett.120.141103](https://doi.org/10.1103/PhysRevLett.120.141103)
- . 2022, *Nature Phys.*, 18, 112, doi: [10.1038/s41567-021-01425-7](https://doi.org/10.1038/s41567-021-01425-7)
- Goldstein, A., Veres, P., Burns, E., et al. 2017, *The Astrophysical Journal Letters*, 848, L14
- Green, S. R., Simpson, C., & Gair, J. 2020, *Phys. Rev. D*, 102, 104057, doi: [10.1103/PhysRevD.102.104057](https://doi.org/10.1103/PhysRevD.102.104057)
- Heaton, J. 2018, *Genetic Programming and Evolvable Machines*, 19, 305
- Hotokezaka, K., Nakar, E., Gottlieb, O., et al. 2019, *Nature Astron.*, 3, 940, doi: [10.1038/s41550-019-0820-1](https://doi.org/10.1038/s41550-019-0820-1)
- Huber, M. C., & Davis, D. 2022. <https://arxiv.org/abs/2208.13844>
- Huth, S., Pang, P. T., Tews, I., et al. 2022, *Nature*, 606, 276
- Iyer, B., Souradeep, T., Unnikrishnan, C., et al. 2011, URL <https://dcc.ligo.org/cgi-bin/DocDB/ShowDocument>
- Kasliwal, M. M., Kasen, D., Lau, R. M., et al. 2019, *Monthly Notices of the Royal Astronomical Society: Letters*, 510, L7, doi: [10.1093/mnrasl/slz007](https://doi.org/10.1093/mnrasl/slz007)
- Kiendrebeogo, R. W., et al. 2023. <https://arxiv.org/abs/2306.09234>
- Lai, X., Zhou, E., & Xu, R. 2019, *Eur. Phys. J. A*, 55, 60, doi: [10.1140/epja/i2019-12720-8](https://doi.org/10.1140/epja/i2019-12720-8)
- LIGO Scientific Collaboration. 2018, *LIGO Algorithm Library - LALSuite*, free software (GPL), doi: [10.7935/GT1W-FZ16](https://doi.org/10.7935/GT1W-FZ16)
- Macas, R., Pooley, J., Nuttall, L. K., et al. 2022, *Phys. Rev. D*, 105, 103021, doi: [10.1103/PhysRevD.105.103021](https://doi.org/10.1103/PhysRevD.105.103021)
- Margalit, B., & Metzger, B. D. 2017, *The Astrophysical Journal Letters*, 850, L19, doi: [10.3847/2041-8213/aa991c](https://doi.org/10.3847/2041-8213/aa991c)
- Messick, C., Blackburn, K., Brady, P., et al. 2017, *Phys. Rev. D*, 95, 042001, doi: [10.1103/PhysRevD.95.042001](https://doi.org/10.1103/PhysRevD.95.042001)

- Most, E. R., Weih, L. R., Rezzolla, L., & Schaffner-Bielich, J. 2018, *Phys. Rev. Lett.*, 120, 261103, doi: [10.1103/PhysRevLett.120.261103](https://doi.org/10.1103/PhysRevLett.120.261103)
- Nitz, A. H., Dal Canton, T., Davis, D., & Reyes, S. 2018, *Phys. Rev. D*, 98, 024050, doi: [10.1103/PhysRevD.98.024050](https://doi.org/10.1103/PhysRevD.98.024050)
- Nitz, A. H., Kumar, S., Wang, Y.-F., et al. 2023, *Astrophys. J.*, 946, 59, doi: [10.3847/1538-4357/aca591](https://doi.org/10.3847/1538-4357/aca591)
- Pan, S. J., & Yang, Q. 2009, *IEEE Transactions on knowledge and data engineering*, 22, 1345
- Pankow, C., Rizzo, M., Rao, K., Berry, C. P. L., & Kalogera, V. 2020, *Astrophys. J.*, 902, 71, doi: [10.3847/1538-4357/abb373](https://doi.org/10.3847/1538-4357/abb373)
- Pankow, C., et al. 2018, *Phys. Rev. D*, 98, 084016, doi: [10.1103/PhysRevD.98.084016](https://doi.org/10.1103/PhysRevD.98.084016)
- Petrov, P., Singer, L. P., Coughlin, M. W., et al. 2022, *The Astrophysical Journal*, 924, 54
- Pian, E., et al. 2017, *Nature*, 551, 67, doi: [10.1038/nature24298](https://doi.org/10.1038/nature24298)
- Powell, J. 2018, *Class. Quant. Grav.*, 35, 155017, doi: [10.1088/1361-6382/aacf18](https://doi.org/10.1088/1361-6382/aacf18)
- Powell, J., Sun, L., Gereb, K., Lasky, P. D., & Dollmann, M. 2023, *Class. Quant. Grav.*, 40, 035006, doi: [10.1088/1361-6382/acb038](https://doi.org/10.1088/1361-6382/acb038)
- Radice, D., et al. 2018, *Astrophys. J. Lett.*, 852, L29, doi: [10.3847/2041-8213/aaa402](https://doi.org/10.3847/2041-8213/aaa402)
- Raza, N., Chan, M. L., Haggard, D., et al. 2024, *The Astrophysical Journal*, 963, 98, doi: [10.3847/1538-4357/ad13ea](https://doi.org/10.3847/1538-4357/ad13ea)
- Rosswog, S., Feindt, U., Korobkin, O., et al. 2017, *Class. Quant. Grav.*, 34, 104001, doi: [10.1088/1361-6382/aa68a9](https://doi.org/10.1088/1361-6382/aa68a9)
- Savchenko, V., Ferrigno, C., Kuulkers, E., et al. 2017, *The Astrophysical Journal Letters*, 848, L15
- Singer, L. P., & Price, L. R. 2016, *Phys. Rev. D*, 93, 024013, doi: [10.1103/PhysRevD.93.024013](https://doi.org/10.1103/PhysRevD.93.024013)
- Singer, L. P., Chen, H.-Y., Holz, D. E., et al. 2016, *The Astrophysical Journal Letters*, 829, L15, doi: [10.3847/2041-8205/829/1/L15](https://doi.org/10.3847/2041-8205/829/1/L15)
- Smartt, S. J., et al. 2017, *Nature*, 551, 75, doi: [10.1038/nature24303](https://doi.org/10.1038/nature24303)
- Tsukada, L., Joshi, P., Adhicary, S., et al. 2023, *Phys. Rev. D*, 108, 043004, doi: [10.1103/PhysRevD.108.043004](https://doi.org/10.1103/PhysRevD.108.043004)
- Watson, D., et al. 2019, *Nature*, 574, 497, doi: [10.1038/s41586-019-1676-3](https://doi.org/10.1038/s41586-019-1676-3)
- Zevin, M., Coughlin, S., Bahaadini, S., et al. 2017, *Classical and Quantum Gravity*, 34, 064003, doi: [10.1088/1361-6382/aa5cea](https://doi.org/10.1088/1361-6382/aa5cea)
- Zevin, M., et al. 2023. <https://arxiv.org/abs/2308.15530>